

Field Dependent Surface Magnetism in $\text{La}_{1.2}\text{Sr}_{1.8}\text{Mn}_2\text{O}_7$

Benjamin Bryant,^{1,2} Y. Moritomo,³ Y. Tokura,^{4,5,6} and G. Aeppli¹

¹*London Centre for Nanotechnology and Department of Physics and Astronomy,
University College London, London WC1E 6BT, UK*

²*present address: Delft University of Technology, Kavli Institute of Nanoscience,
Department of Quantum Nanoscience, Lorentzweg 1, 2628 CJ Delft, The Netherlands*

³*Graduate School of Pure and Applied Science, University of Tsukuba, Tsukuba, Ibaraki 305-8571, Japan*

⁴*Multiferroic Project, ERATO, Japan Science and Technology Agency (JST), Wako, 351-0198, Japan*

⁵*Cross-Correlated Materials Research Group (CMRG),*

RIKEN, Advanced Science Institute, Wako, 351-0198, Japan

⁶*Department of Applied Physics, University of Tokyo, Bunkyo-ku, Tokyo 113-8656, Japan*

(Dated: January 27, 2023)

Colossal magnetoresistance and field-induced ferromagnetism are well documented in manganite compounds. Since domain wall resistance may contribute to magnetoresistance, data on the temperature and magnetic field dependence of the ferromagnetic domain structure are required for a full understanding of the magnetoresistive effect. Here we show, using cryogenic Magnetic Force Microscopy, domain structures for the layered manganite $\text{La}_{1.2}\text{Sr}_{1.8}\text{Mn}_2\text{O}_7$ as a function of temperature and magnetic field. Surface Bloch walls appear to be suppressed close to T_C : domain walls may be resolved either by the application of a c-axis magnetic field, or by decreasing the temperature further, indicating a temperature-dependent magnetic anisotropy. Magnetic structures are seen also at temperatures well above T_C : these features are attributed to inclusions of additional Ruddleson-Popper manganite phases. Low-temperature domain walls are nucleated by these ferromagnetic inclusions.

Many manganite compounds exhibit the property of negative colossal magnetoresistance (CMR), a very large reduction in electrical resistance upon application of a magnetic field [1]. Bilayer manganites exhibit colossal magnetoresistance in a similar way to the cubic compounds [2]: the effect is considerably larger than in cubic crystals having the same cation doping, implying that the CMR effect is enhanced by the bilayer structure [3]. In all cases the largest magnetoresistance is found at temperatures close to the metal-insulator transition, which is attendant on the Curie transition. A simple phenomenological explanation for CMR is as an effect of spin disorder close to T_C . This disorder can be suppressed by an applied magnetic field, enhancing the double-exchange hopping probability and hence the conductivity [1]. Effectively, the magnetic field has shifted the Curie and metal-insulator transition to a higher temperature.

This simple explanation is obviously not sufficient: a complete model of colossal magnetoresistance in manganites must take into account effects such as phase separation [4]: recently, the evolution of ferromagnetic metal regions in an insulating matrix in a CMR manganite has been studied in great detail [5]. The existence of impurity phases with higher T_C to the bulk will be critical for colossal magnetoresistance, as these will act as nucleation sites for the field-induced ferromagnetic phase. Ferromagnetic domain walls contribute to magnetoresistance in manganites [6, 7], particularly in ultra-thin films [8]: domain wall resistance may play a similar role in the quasi-two-dimensional layered manganites. For a complete understanding of magnetoresistance in layered manganites therefore, it is desirable that

ferromagnetic domains be imaged both in the zero field low temperature state and in the field-induced ferromagnetic state. To this end, we present here low-temperature Magnetic Force Microscopy (MFM) data for a CMR ferromagnetic bilayered manganite. Bilayered manganites - $\text{La}_{2-2x}\text{Sr}_{1+2x}\text{Mn}_2\text{O}_7$, where x is the cation doping - provide an opportunity to obtain good-quality surfaces,

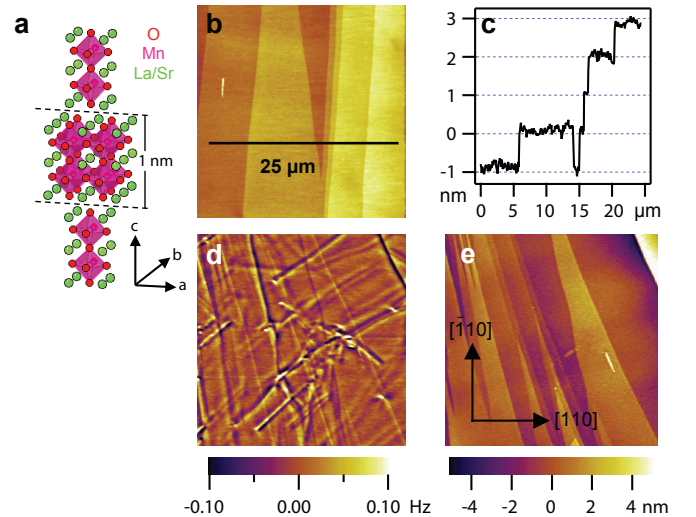


FIG. 1. (color online). (a) Crystal structure of $\text{La}_{1.2}\text{Sr}_{1.8}\text{Mn}_2\text{O}_7$ (b) Room temperature AFM topograph. The scale line shows the location of the cross section (c). Terrace step heights are always $c/2 = 1$ nm or multiples thereof. (d) $25 \times 25 \mu\text{m}$ MFM image collected at 4.7 K, showing domain walls. (e) corresponding AFM topographic image.

as these compounds may be readily cleaved to provide a clean, atomically flat surface [9–11]. Previous spatially-resolved magnetic studies on bilayered manganites have included spin-polarized SEM on antiferromagnetic [12] and ferromagnetic [13] layered manganites, and MFM on the ferromagnet $\text{La}_{1.36}\text{Sr}_{1.64}\text{Mn}_2\text{O}_7$ ($x=0.32$) [14].

For the current study the bilayer compound $\text{La}_{1.2}\text{Sr}_{1.8}\text{Mn}_2\text{O}_7$ ($x=0.4$), was selected (figure 1a): at this doping, the material is known to exhibit colossal magnetoresistance [3]. Single crystal samples were grown by an optical float zone method. Preliminary room-temperature AFM scans were carried out on $\text{La}_{1.2}\text{Sr}_{1.8}\text{Mn}_2\text{O}_7$ crystals, cleaved in air: figure 1b shows a typical AFM topograph. The surface is largely clean and exhibits a roughness of < 0.1 nm: large terraces up to $10\text{ }\mu\text{m}$ across are observed. Terrace steps are always 1.0 ± 0.1 nm, or multiples thereof, corresponding to $c/2 = 1.007$ nm [3].

Magnetic Force Microscopy measurements were carried out using an Attocube low-temperature AFM, in the temperature range 4.2 K to room temperature. The AFM was operated in Helium exchange gas, in frequency modulation mode. MFM images were obtained in units of frequency shift, $\Delta f \propto -\delta F_z/\delta z$, where F_z is the z-component of the magnetic force between the tip and the sample stray field. Commercial MFM probes were used, with moment $\approx 0.3 \times 10^{-13}$ e.m.u: the MFM lift height was 50 nm. A magnetic field of up to 8 T was applied, in the c-axis direction. $\text{La}_{1.2}\text{Sr}_{1.8}\text{Mn}_2\text{O}_7$ single crystal samples were cleaved in air before being loaded into the low-temperature AFM. Bulk magnetization measurements were also carried out, using a SQUID magnetometer.

Figure 1d shows an MFM image of $\text{La}_{1.2}\text{Sr}_{1.8}\text{Mn}_2\text{O}_7$ collected at 4.7 K, showing the ferromagnetic domain structure. Some crosstalk may be seen between the magnetic and topographic (figure 1e) images, but the magnetic features are readily distinguished from terrace edges. The easy axis of magnetization is in the ab plane [15, 16], so since the MFM tip is magnetized in the c-axis direction the magnetic contrast seen here is due to Bloch-type domain walls. Linear domain walls are observed, with an average spacing of $\approx 5\text{ }\mu\text{m}$: domain walls are observed to cross terrace edges, and are not aligned to the crystallographic axes. The presence of a domain state in $\text{La}_{1.2}\text{Sr}_{1.8}\text{Mn}_2\text{O}_7$ below T_C was predicted by Potter et al. [17]. Figure 2 shows a variable-temperature MFM study: the same area is imaged at 80 K, 95 K and 100 K. At 80 K the domain walls are clear: at 95 K the domain walls are still visible, but with reduced contrast: by 100 K the domains are no longer visible. The remaining contrast at 100 K is due to topographic features (terrace edges). Figure 2e shows the domain wall contrast, quantified as the peak to peak amplitude of the magnetic image, as a function of temperature in the range 50 K to 150 K. The effect of the topographic features on the measured am-

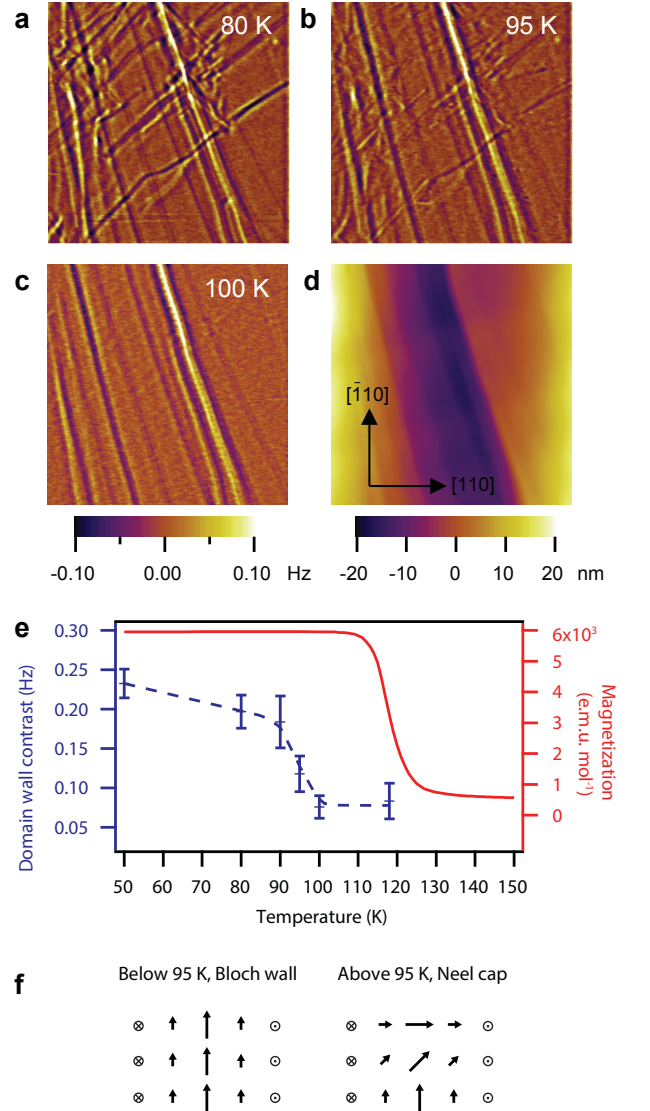


FIG. 2. (color online). (a - d) $26 \times 26\text{ }\mu\text{m}$ MFM images at 80 K (a), 95 K (b) and 100 K (c). Domain walls, visible at 80 K have disappeared at 100 K, leaving only topographic features. (d) AFM topographic image. (e) Comparison of bulk magnetization ($H=100$ Oe \parallel ab) and surface domain wall contrast as observed by MFM: the dashed line is a guide to the eye. A steep drop in the visibility of domain walls is seen at 95 K, well below the bulk $T_C = 118$ K. (f) Schematic of Bloch walls vs. domain walls with surface Neel cap: the Neel cap results in a much smaller stray field and hence MFM signal.

plitude has been eliminated by measuring sections parallel to the terrace edges. Bulk magnetization in the same temperature range is also shown. The Curie temperature may be measured from the minimum in dM/dT as $T_C = 118$ K: the domain wall contrast however shows a sharp drop at a considerably lower temperature, around 95 K. In previous MFM studies, domain wall contrast has been observed to increase with decreasing temperature below

T_C [18–20], however these studies show a linear increase in contrast, rather than the sharp jump observed here.

Several explanations might be advanced for the suppression of domain wall contrast above 95 K: (1) a bulk spin reorientation transition, (2) a magnetic ‘dead’ layer close to T_C , (3) a transition from surface Bloch domain walls to Neél capped walls as a result of a temperature dependent magnetic anisotropy.

A spin reorientation transition has been proposed in $\text{La}_{1.2}\text{Sr}_{1.8}\text{Mn}_2\text{O}_7$ on the basis of neutron diffraction experiments [21], with spins rotating from the c -axis to close to the ab plane on cooling from 130 K to 100 K: this might explain the change in magnetic imaging near 95 K. A spin reorientation transition with temperature is observed in $\text{La}_{1.36}\text{Sr}_{1.64}\text{Mn}_2\text{O}_7$ ($x=0.32$): MFM studies [14] show a clear change from domain imaging (spins in c -axis) to imaging domain walls (spins in ab plane). Such a change is not seen here for $\text{La}_{1.2}\text{Sr}_{1.8}\text{Mn}_2\text{O}_7$: the same type of domain structure is observed at all temperatures, so we may rule out a spin reorientation transition as an explanation for the suppressed domain wall contrast.

Magnetic tunnel junction measurements [22–25] and spin-polarized photoemission spectroscopy [26] indicate the existence close to T_C of a subsurface ‘dead’ layer with reduced spin polarization a few nm thick. In bilayer manganites an abrupt interface between the ferromagnetic bulk state and a non-ferromagnetic surface layer one bilayer (1 nm) thick has been identified, via X-ray resonant magnetic scattering (XRMS) [27, 28]. In general however the thickness of any magnetic dead layer is far less than the typical MFM lift height of 50 nm: we would certainly expect to be able to resolve domain walls via MFM in the presence of a magnetically dead surface layer a few nm thick, suggesting that this effect cannot explain the non-observation of domain walls at $T \geq 100$ K.

The final possible explanation for the suppressed domain wall contrast lies with the fact that, although the bulk domain walls are Bloch-type, near the surface the wall may transition to a Neél wall, i.e. a Neél cap: this is shown schematically in figure 2f. The length scale of the transition has been found to be similar to the domain wall width [29]. The Neél cap minimizes the stray field at the domain wall, implying a much reduced MFM contrast. We conclude that the drop off in domain wall contrast above 95 K represents a transition from Bloch-terminated to Neél terminated domain walls, implying a decrease in magnetic anisotropy with increasing temperature when approaching T_C .

Due to the CMR effect, $\text{La}_{1.2}\text{Sr}_{1.8}\text{Mn}_2\text{O}_7$ exhibits an effective shift of T_C to higher temperature upon application of a magnetic field (see supplementary figure S1). We predict therefore that, in the temperature range $95 \text{ K} < T < T_C$, domain wall contrast will re-emerge with the application of field. To this end magnetic field dependent MFM imaging was carried out at 118 K and 100 K. Fig-

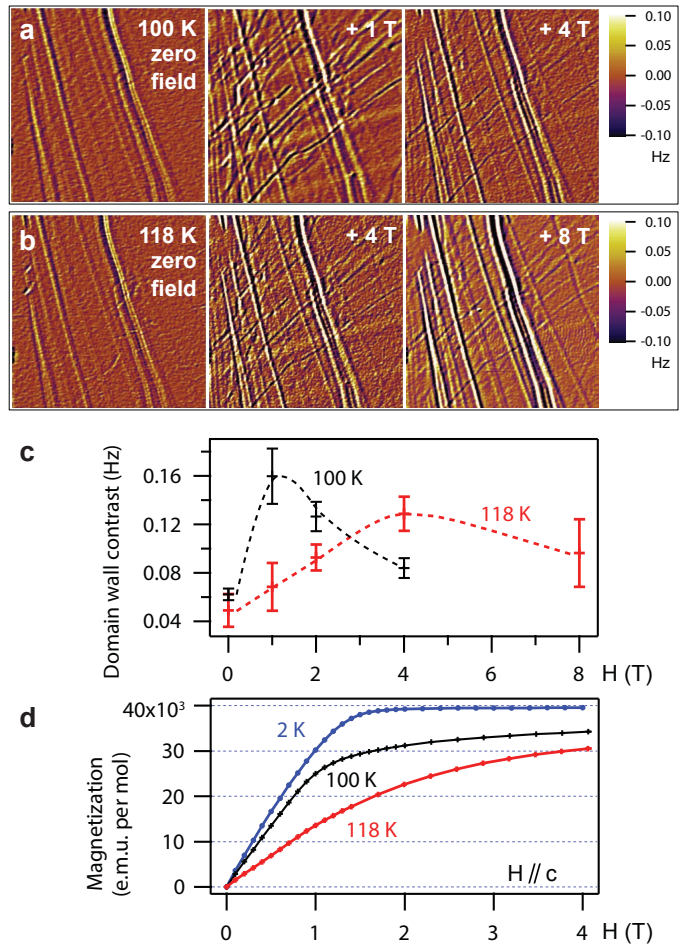


FIG. 3. (color online). (a) Field dependence of MFM imaging at 100 K: the area is the same as for figure 2c. (b) Field dependence of MFM imaging at 118 K: the area is the same as (a). All MFM images are $26 \times 26 \mu\text{m}$ (c) Domain wall contrast as a function of field for 100 K and 118 K. Dashed lines are guides to the eye (d) Bulk magnetization vs. applied field ($H \parallel c$) for 2 K, 100 K and 118 K. Neither MFM data nor M vs. H have been corrected for the demagnetizing field, though both samples have a similar aspect ratio.

ure 3a shows the results of field-dependent MFM measurements at 100 K. The scan area is the same as in figure 2a: the field is applied along the c -axis. At zero field no domains are observed: under an applied field of 1 T domains similar to the low-temperature state become visible. At higher fields (up to 4 T) the domains become less clear, as the sample becomes magnetized. Figure 3b shows the field dependence of MFM imaging at 118 K. The result is similar to 100 K, but a much larger field is needed in order to make the domains visible, with peak domain contrast at 4 T. Figure 3c summarizes the field dependence of the domain wall contrast, quantified as the peak to peak amplitude of the magnetic image, for 100 K and 118 K. By comparison of figure 3a to 2a we may observe that domain walls form in the same configu-

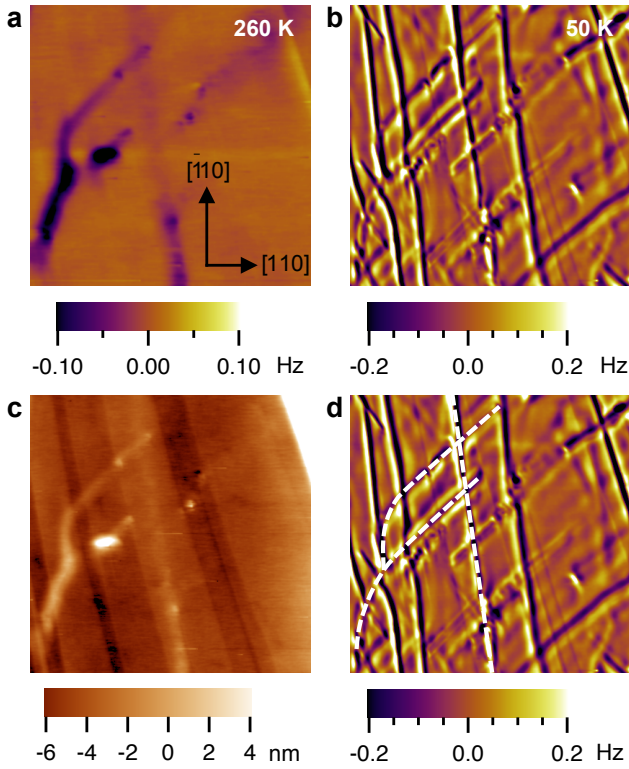


FIG. 4. (color online). Magnetic contrast above and below T_C (a) $15 \times 15 \mu\text{m}$ MFM image at 260 K (b) same area at 50 K. (c) Topographic image at 260 K of same area as (a) and (b), showing terraces edges, and also some crosstalk from the magnetic image. (d) Same as (b): dashed lines highlight magnetic features which persist above and below T_C .

ration under application of a field, as if the temperature is decreased.

We conclude that, for $95 \text{ K} < T < T_C$, Néel - terminated domain walls are converted to Bloch walls by the application of a c -axis field. In the current experiment, because the field is applied perpendicular to the easy axis of magnetization, the energy to form Bloch walls is reduced by an applied field. This may be demonstrated by the formation of new domain walls under applied field (see supplementary figure S2). Above a certain critical field the sample starts to become magnetized, and the domain contrast starts to decrease again, as shown in figure 3c. At both 100 K and 118 K the field-induced domain structure observed by MFM has maximum contrast when the sample magnetization has reached around 75 % of the saturation value (figure 3d).

In a minority of locations on the $\text{La}_{1.2}\text{Sr}_{1.8}\text{Mn}_2\text{O}_7$ surface, magnetic image features are observed even well above $T_C = 118 \text{ K}$. Figure 4a and b show MFM images of the same area both above and below T_C , at 260 K and 50 K. Magnetic features are observed at 260 K as elongated structures $1\text{-}2 \mu\text{m}$ wide. Some crosstalk from the magnetic image can be seen in the topographic image

(figure 4c). The features seen in 4a can however be positively identified as magnetic in origin by comparison with the topographic image, since step edges seen in 4c are not seen in the MFM image. The low temperature domains seen in figure 4b have a similar structure to other areas, which do not show high-temperature magnetic structure, for example figure 1d. By comparison of the MFM images at 260 K and 50 K, it is clear that some magnetic features persist through T_C : figure 4d highlights these features. Domain walls at 50 K are observed to form either as extensions of the magnetic features at 260 K or parallel to these features, suggesting that the low temperature domains are nucleated by the high temperature magnetic features.

The presence of an impurity phase with a higher Curie temperature in $\text{La}_{1.2}\text{Sr}_{1.8}\text{Mn}_2\text{O}_7$ may be inferred from bulk magnetization data. In addition to the bulk Curie transition at $T_C = 118 \text{ K}$, further higher temperature transitions are observed at $T_1 = 245 \text{ K}$, $T_2 = 285 \text{ K}$ and $T_3 = 335 \text{ K}$ (supplementary figure S3). In previous studies [17, 30, 31] such transitions at $T > T_C$ have been attributed to intergrowths of $n > 2$ variants of the Ruddleson-Popper series $\text{La}_{n-nx}\text{Sr}_{1+nx}\text{Mn}_n\text{O}_{3n+1}$. In general, for more three-dimensional compounds (higher n), T_C is higher: the cubic compound ($n = \infty$, $\text{La}_{0.6}\text{Sr}_{0.4}\text{MnO}_3$) has $T_C = 361 \text{ K}$ [3]. It is likely that the additional transitions at T_1 , T_2 and T_3 represent different classes of inclusions with progressively higher n . The ratio of the saturation moment of the ferromagnetic component at $T > T_C$ to the saturation moment at $T < T_C$ [31], allows the volume fraction of inclusions to be estimated at 1.5 % (supplementary figure S3). The presence of $n > 2$ impurity phases provides an explanation for the observation of magnetic features at $T > T_C$: magnetic features in images such as figure 4a indicate the location of such ferromagnetic inclusions. As the material is cooled below T_C these inclusions act as nucleation points for the formation of domain walls.

In summary, we observe that in the colossal magnetoresistive layered manganite $\text{La}_{1.2}\text{Sr}_{1.8}\text{Mn}_2\text{O}_7$, Bloch-type domain walls are converted to Néel capped walls close to T_C . The application of a c -axis magnetic field, smaller than the saturation field, re-establishes the Bloch walls. We anticipate that this effect will have an impact on colossal magnetoresistance, due to the influence of domain wall resistance [6–8]. Inclusions of $n > 2$ Ruddleson-Popper phases in the layered material have been identified by magnetic imaging, since their transition temperatures are much higher than the bulk T_C . Upon cooling through T_C , domain walls are nucleated by these ferromagnetic inclusions. Low-temperature MFM provides an ideal method to study magnetic phase inclusions and nucleation processes, both of which are crucial to a proper understanding of the phenomenon of colossal magnetoresistance.

-
- [1] Y. Tokura, Reports on Progress in Physics **69**, 797 (2006).
- [2] T. Kimura and Y. Tokura, Annual Review of Materials Science **30**, 451 (2000).
- [3] Y. Moritomo, A. Asamitsu, H. Kuwahara, and Y. Tokura, Nature **380**, 141 (1996).
- [4] E. Dagotto, T. Hotta, and A. Moreo, Physics Reports **344**, 1 (2001).
- [5] Y. Murakami, H. Kasai, J. J. Kim, S. Mamishin, D. Shindo, S. Mori, and A. Tonomura, Nat Nano **5**, 37 (2010).
- [6] Y. Wu, Y. Suzuki, U. Rudiger, J. Yu, A. D. Kent, T. K. Nath, and C. B. Eom, Applied Physics Letters **75**, 2295 (1999).
- [7] N. D. Mathur, G. Burnell, S. P. Isaac, T. J. Jackson, B. S. Teo, J. L. MacManus-Driscoll, L. F. Cohen, J. E. Evetts, and M. G. Blamire, Nature **387**, 266 (1997).
- [8] Q. Li, Y. F. Hu, and H. S. Wang, Journal of Applied Physics **89**, 6952 (2001).
- [9] H. Ronnow, C. Renner, G. Aeppli, T. Kimura, and Y. Tokura, Nature **440**, 1025 (2006).
- [10] B. Bryant, C. Renner, Y. Tokunaga, Y. Tokura, and G. Aeppli, Nature Communications **2** (2011), 10.1038/ncomms1219.
- [11] F. Massee, S. de Jong, Y. Huang, W. K. Siu, I. Santoso, A. Mans, A. T. Boothroyd, D. Prabhakaran, R. Follath, A. Varykhalov, L. Patthey, M. Shi, J. B. Goedkoop, and M. S. Golden, Nat Phys **7**, 978 (2011).
- [12] M. Konoto, T. Kohashi, K. Koike, T. Arima, Y. Kaneko, T. Kimura, and Y. Tokura, Physical Review Letters **93** (2004), 10.1103/PhysRevLett.93.107201.
- [13] M. Konoto, T. Kohashi, K. Koike, T. Arima, Y. Kaneko, T. Kimura, and Y. Tokura, Physical Review B **71** (2005), 10.1103/PhysRevB.71.184441.
- [14] J. Huang, C. Hyun, T.-M. Chuang, J. Kim, J. B. Goodenough, J. S. Zhou, J. F. Mitchell, and A. de Lozanne, Phys. Rev. B **77** (2008), 10.1103/PhysRevB.77.024405.
- [15] K. Hirota, Y. Moritomo, H. Fujioka, M. Kubota, H. Yoshizawa, and Y. Endoh, J. Phys. Soc. Jpn. **67**, 3380 (1998).
- [16] M. Kubota, H. Fujioka, K. Ohoyama, K. Hirota, Y. Moritomo, H. Yoshizawa, and Y. Endoh, Journal of Physics and Chemistry of Solids **60**, 1161 (1999).
- [17] C. Potter, M. Swiatek, S. Bader, D. Argyriou, J. Mitchell, D. Miller, D. Hinks, and J. Jorgensen, Physical Review B **57**, 72 (1998).
- [18] Y. Soh, G. Aeppli, N. Mathur, and M. Blamire, Journal of Magnetism and Magnetic Materials **226**, 857 (2001).
- [19] Y. Ma, C. Chueh, W. Kuang, Y. Liou, and Y. Yao, Journal of Magnetism and Magnetic Materials **239**, 371 (2002).
- [20] Q. Lu, C. Chen, and A. de Lozanne, Science **276**, 2006 (1997).
- [21] Y. Choi, S. Kim, Y. Kwon, C. Lee, J. Lee, and H. Shim, Journal of the Korean Physical Society **42**, 522 (2003).
- [22] M. Viret, J. Nassar, M. Drouet, J. Contour, C. Fermon, and A. Fert, Journal of Magnetism and Magnetic Materials **198-199**, 1 (1999).
- [23] M. Bowen, M. Bibes, A. Barthelemy, J.-P. Contour, A. Anane, Y. Lemaitre, and A. Fert, Applied Physics Letters **82**, 233 (2003).
- [24] T. Obata, T. Manako, Y. Shimakawa, and Y. Kubo, Applied Physics Letters **74**, 290 (1999).
- [25] C. Kwon, Q. X. Jia, Y. Fan, M. F. Hundley, D. W. Reagor, J. Y. Coulter, and D. E. Peterson, Applied Physics Letters **72**, 486 (1998).
- [26] J. H. Park, E. Vescovo, H.-J. Kim, C. Kwon, R. Ramesh, and T. Venkatesan, Phys. Rev. Lett. **81**, 1953 (1998).
- [27] J. Freeland, K. Gray, L. Ozyuzer, P. Berghuis, E. Badica, J. Kavich, H. Zheng, and J. Mitchell, Nature Materials **4**, 62 (2005).
- [28] J. Freeland, J. Kavich, K. Gray, L. Ozyuzer, H. Zheng, J. Mitchell, M. Warusawithana, P. Ryan, X. Zhai, R. Kodama, and J. Eckstein, Journal of Physics Condensed Matter **19** (2007), 10.1088/0953-8984/19/31/315210.
- [29] M. R. Scheinfein, J. Unguris, J. L. Blue, K. J. Coakley, D. T. Pierce, R. J. Celotta, and P. J. Ryan, Physical Review B **43**, 3395 (1991).
- [30] G. Allodi, M. Bimbi, R. De Renzi, C. Baumann, M. Apostu, R. Suryanarayanan, and A. Revcolevschi, Physical Review B **78**, 064420 (2008).
- [31] S. Bader, R. Osgood, D. Miller, J. Mitchell, and J. Jiang, Journal of Applied Physics **83**, 6385 (1998).